

**Impact of Mono-Fluorination on the Photophysics of the Flavin Chromophore:
A Quantum Chemical Perspective
(Electronic Supplementary information)**

*Mario Bracker, Fabian Dinkelbach, Oliver Weingart, Martin Kleinschmidt**

Institute of Theoretical and Computational Chemistry, Heinrich Heine University Düsseldorf, Universitätsstr. 1,
D-40225 Düsseldorf, Germany

Corresponding author

*Tel.: +49 211 8113209; fax: +49 211 8113466.
E-mail address: Martin.Kleinschmidt@uni-duesseldorf.de (M. Kleinschmidt).
URL: <http://www.theochem.uni-duesseldorf.de> (M. Kleinschmidt).

1 Molecular orbitals

At the ground state geometries the energetic order of orbitals in general is as follows:

1. π_{L+2}

2. π_{L+1}

3. π_L

4. π_H

5. π_{H-1}

6. n_{O2}

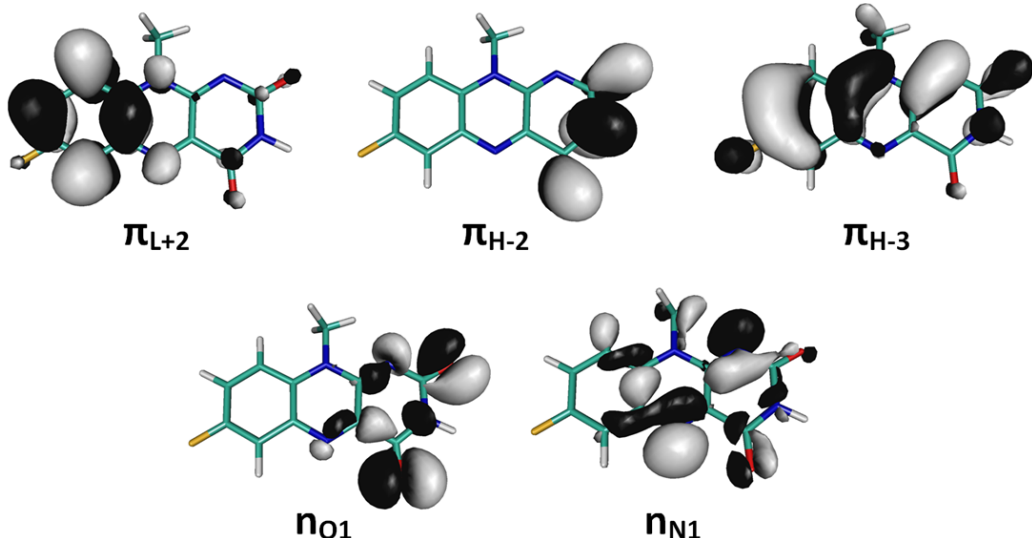
7. π_{H-2}

8. n_{N2}

9. n_{O1}

10. π_{H-3}

11. n_{N1}



The remaining orbitals of 7F-MIA are depicted in the main paper. With respect to the O/N2 orbitals, the O/N1 orbitals in large part represent the opposite linear combinations of the respective in-plane lone pairs.

2 Geometries

2.1 Ground state

Table S1: Calculated bond lengths in picometres (pm) for the ground state of MIA and its fluorinated derivatives 6-9F-MIA. Experimental values originate from X-ray diffraction [M. Wang, C. J. Fritchie Jr., Acta Crystallogr. (1973) 2040-2045].

Bond	Length / pm					
	MIA	exp.	6F-MIA	7F-MIA	8F-MIA	9F-MIA
N(1)-C(2)	138.1	136.0(5)	138.3	138.2	138.3	138.2
C(2)-N(3)	141.4	140.8(5)	141.3	141.5	141.3	141.4
N(3)-C(4)	137.9	135.4(5)	138.0	137.8	137.9	137.7
C(4)-C(4a)	150.2	148.5(5)	150.3	150.4	150.1	150.4
C(4a)-N(5)	129.0	129.5(5)	129.0	129.0	129.1	128.8
N(5)-C(5a)	136.9	136.6(5)	136.3	137.0	136.6	136.9
C(5a)-C(6)	140.6	141.8(5)	141.1	140.5	140.6	140.5
C(6)-C(7)	137.8	136.8(6)	137.5	137.2	137.7	137.6
C(7)-C(8)	140.1	139.5(6)	139.8	139.4	139.5	139.8
C(8)-C(9)	138.4	138.8(6)	138.4	138.3	137.9	137.7
C(9)-C(9a)	140.3	139.2(5)	140.3	140.4	140.2	140.8
C(9a)-N(10)	138.6	139.0(5)	138.4	138.6	138.2	138.8
N(10)-C(10a)	138.2	136.9(5)	138.4	138.1	138.5	138.6
C(10a)-N(1)	130.0	131.9(5)	129.8	129.9	129.8	129.9
C(5a)-N(9a)	141.9	141.8(5)	142.0	141.8	141.7	142.4
C(4a)-N(10a)	146.2	146.6(5)	146.2	146.3	146.1	146.1
C(10)-R	146.8	148.8(5)	146.8	146.8	146.8	147.9
C(2)-O	121.1	121.6(5)	121.0	121.1	121.0	121.0
C(4)-O	121.0	121.7(5)	120.9	121.0	121.0	121.0
C(6/7/8/9)-F	-	-	133.4	134.8	134.5	135.4

2.2 Excited states

Table S2: Calculated bond lengths in picometres (pm) for the excited states (S1, S2, T1-3) of 7F-MIA.

Bond	Length / pm				
	S1	S2	T1	T2	T3
N(1)-C(2)	140.2	130.5	139.3	137.7	138.1
C(2)-N(3)	137.7	135.9	138.4	140.3	140.9
N(3)-C(4)	141.5	143.3	139.9	138.8	138.7
C(4)-C(4a)	145.6	145.2	147.3	146.2	147.0
C(4a)-N(5)	135.2	135.5	136.2	132.2	136.8
N(5)-C(5a)	134.1	133.6	133.5	134.5	132.5
C(5a)-C(6)	140.8	142.0	141.6	139.9	144.1
C(6)-C(7)	138.0	136.9	136.8	137.9	142.9
C(7)-C(8)	139.9	139.5	140.6	138.5	135.3
C(8)-C(9)	138.6	139.0	138.3	139.4	144.5
C(9)-C(9a)	140.3	139.4	140.1	139.3	139.7
C(9a)-N(10)	138.8	140.2	138.6	140.1	138.0
N(10)-C(10a)	137.2	136.4	140.2	138.5	141.1
C(10a)-N(1)	133.2	135.5	132.5	130.0	130.3
C(5a)-N(9a)	144.7	143.6	145.7	142.8	142.8
C(4a)-N(10a)	142.9	141.1	141.0	144.5	142.8
C(10)-R	147.1	146.5	146.4	146.4	146.5
C(2)-O	121.8	129.3	121.9	121.2	121.4
C(4)-O	121.5	121.0	121.3	121.8	121.9
C(7)-F	134.1	135.1	134.3	134.8	133.9

3 Solvent modeling

Table S3 summarizes statistics derived from overall 50 molecular dynamics simulations, which were conducted to ensure a systematic approach for including explicit interactions of the investigated flavins with water (solvation model B).

Table S3: Count of hydrogen bridge linkages per oxygen/nitrogen/fluorine atom for MIA and its fluorinated (positions 6-9) derivatives. In the last two columns the counts C and relative frequencies $f_{\text{rel.}}$ are specified. The results stem from QM/MM-optimized snapshots of molecular dynamics simulations at 298 K and 1 bar, each lasting for 200 ps.

Atom	Count of hydrogen bridge linkages					C	$f_{\text{rel.}}$
	MIA	6F-MIA	7F-MIA	8F-MIA	9F-MIA		
N(1)	8	8	10	6	9	41	0.82
O(11)	20	19	20	21	19	99	1.98
N(3)	11	9	9	10	9	48	0.96
O(13)	15	17	12	15	13	72	1.44
N(5)	4	5	6	4	6	25	0.50
F(6/7/8/9)	-	3	5	4	5	17	0.43

4 Vibronic absorption spectra

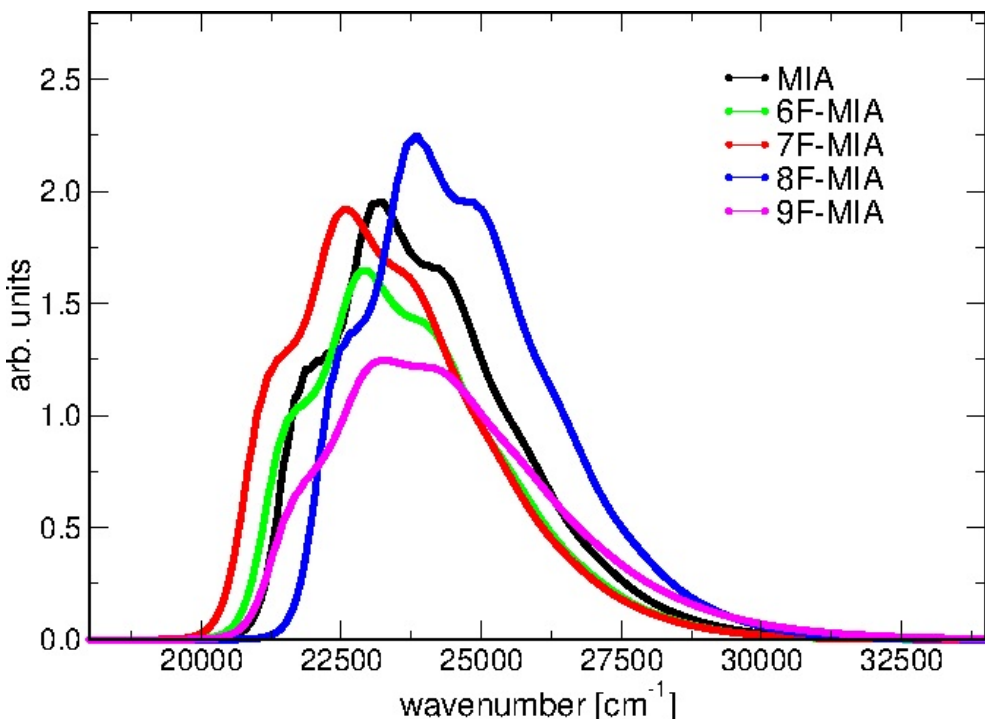


Figure S1: DFT/MRCI computed (model A) vibronic absorption spectra highlighting vibrational finestructure.

5 Artificial imaginary frequencies

To obtain real-valued values for artificial imaginary frequencies we carried out least square fits for TDDFT scans along the respective modes – the convoluted potential stemming from the artifact

herefore was excluded. In practice we neglected the inner region of the respective parabola: Beginning at the artificial maximum points were neglected consecutively until a threshold for the coefficient of determination fulfilled a criterion of $R^2 > 0.9999$. To validate this approach, the same procedure was tested for normal modes delivering real-valued frequencies with respect to normal mode analysis – the resulting frequencies were reproduced well for fitted parabolas neglecting the inner region of the fitted curves.

6 Adiabatic transition energies

Gas phase

To construct potential relaxation paths after photoexcitation, adiabatic transition energies are indispensable. Table S4 summarizes those for the S1 minima to the respective triplet minima T1, T2 and T3 of MIA and its derivatives 6F-, 7F, 8F- and 9F-MIA in gas phase. This selection is due to the preferential population of the comparatively long-lived S1 state with regard to the absorption-relaxation-cycle.

Table S4: Summarized adiabatic transition energies in gas phase. The values include zero-point vibrational energy (ZPVE) corrections for the equilibrium geometries. Computed ISC rate constants are given in brackets.

Flavin	Energy difference / eV; (rate constant / s ⁻¹)				
	adiabatic transition				
	S1 \rightsquigarrow T1	S1 \rightsquigarrow T2	S1 \rightsquigarrow T3	S1 \rightsquigarrow S0	S1 \rightsquigarrow S2
MIA	-0.64 (1.4 · 10 ⁷)	-0.06 (2.3 · 10 ⁹)	0.09	-2.59	0.27
6F-MIA	-0.64 (1.5 · 10 ⁷)	-0.06 (3.7 · 10 ⁹)	0.06	-2.60	0.28
7F-MIA	-0.65 (8.6 · 10 ⁶)	-0.02 (1.3 · 10 ⁹)	0.15	-2.52	0.27
8F-MIA	-0.68 (5.8 · 10 ⁶)	-0.08 (2.9 · 10 ⁹)	0.13	-2.66	0.17
9F-MIA	-0.63 (1.5 · 10 ⁷)	-0.06 (2.2 · 10 ⁹)	0.00	-2.57	0.31

Aqueous medium

For the solvated flavins the energetics of the S1 and T1 states and as a consequence S1 \rightsquigarrow T1 transition energies barely change. Due to strong stabilization of the T3 state in water, the S1 \rightsquigarrow T3 channel becomes thermodynamically allowed for all vibrational states. Reversely, the T2 state is strongly blue shifted and consequentially can be neglected. Similarly, (nπ*)¹-states are strongly blue shifted in aqueous medium, so that interaction with the S1 potential is excluded from the investigation.

Table S5: Summarized adiabatic transition energies in aqueous solution. The values include zero-point vibrational energy (ZPVE) corrections for the equilibrium geometries. Computed ISC rate constants are given in brackets.

Flavin	Energy difference / eV; (rate constant / s ⁻¹)			
	adiabatic transition			
	S1 ↔ T1	S1 ↔ T2	S1 ↔ T3	S1 ↔ S0
MIA	-0.50 (3.1 · 10 ⁶)	0.11	-0.12 (2.7 · 10 ⁸)	-2.67
6F-MIA	-0.47 (8.2 · 10 ⁶)	0.15	-0.15 (1.6 · 10 ⁸)	-2.63
7F-MIA	-0.52 (3.4 · 10 ⁶)	0.14	-0.02 (2.6 · 10 ⁸)	-2.59
8F-MIA	-0.54 (4.2 · 10 ⁶)	0.05	-0.05 (4.4 · 10 ⁸)	-2.75
9F-MIA	-0.51 (6.1 · 10 ⁶)	0.10	-0.19 (3.2 · 10 ⁸)	-2.66

7 Fluorescence

Table S6: Calculated transition dipole moments μ_{S1S0} in Debye of MIA and its fluorinated derivatives 6F-, 7F-, 8F- and 9F-MIA in gas phase as well as aqueous solution.

Flavin	μ_{S1S0}	
	gas phase	H ₂ O
MIA	4.80	4.54
6F-MIA	4.53	4.24
7F-MIA	4.78	4.65
8F-MIA	5.04	4.81
9F-MIA	4.31	4.09

8 Spin-orbit coupling

For the lowest ($\pi\pi^*$)³-transitions, T1 and T3, direct couplings do not exceed the size of order 10⁻⁴ cm⁻² and a vibronic treatment has to be applied.

8.1 Direct spin-orbit coupling

Table S7: Summary of direct spin-orbit couplings $|\langle \Psi_{S1} | \hat{\mathcal{H}}_{SO} | \Psi_{T2} \rangle|_{q0}^2 / \text{cm}^{-2}$ at the optimized S1 geometries of MIA and its fluorinated derivatives 6F-, 7F-, 8F- and 9F-MIA in gas phase as well as aqueous solution.

Flavin	$ \langle \Psi_{S1} \hat{\mathcal{H}}_{SO} \Psi_{T2} \rangle _{q0}^2$	
	gas phase	H_2O
MIA	77.99	47.78
6F-MIA	109.11	66.01
7F-MIA	66.08	48.49
8F-MIA	74.35	65.94
9F-MIA	71.05	64.24

8.2 Vibronic spin-orbit coupling

The size of derivatives of spin-orbit matrix elements with respect to normal modes Q_k depends on the effectiveness of the respective modes to induce spin-orbit coupling between the involved states. For the investigated transitions, the ${}^3(\pi\pi^*)$ -states (T_1, T_3) are required to borrow $n\pi^*$ -character from triplet states in energetic proximity. Exemplary normal modes for the $S1 \rightsquigarrow T3$ -ISC rate are following a"-modes:

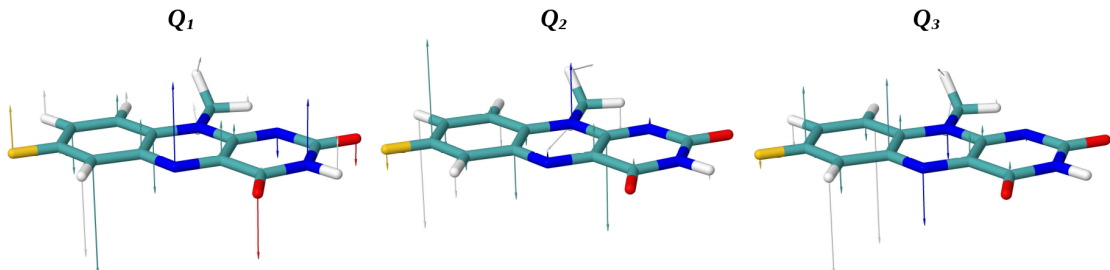


Figure S2: Illustration of three eigenvectors of 7F-MIA.

The depicted eigenvectors induce the biggest derivatives of SOMEs for the considered transition.

Table S8: Biggest derivatives of spin-orbit matrix elements $|\partial \langle \Psi_{S1} | \hat{\mathcal{H}}_{SO} | \Psi_{T3} \rangle|_{q0}^2 / \partial Q_k| / \text{cm}^{-2}$ in water (model A) at the optimized S1 geometry of 7F-MIA with respect to normal modes Q_k and corresponding frequencies $\tilde{\nu} / \text{cm}^{-1}$.

Q_k	$\tilde{\nu}$	$ \partial \text{SOME} / \partial Q_k ^2$
Q_1	147.28	0.42
Q_2	572.88	0.38
Q_3	462.54	0.34

9 Dependency of S1 \rightsquigarrow T3 ISC in water on energy gap

Table S9: Summary of S1 \rightsquigarrow T3 ISC-rate constants in aqueous solution (model A). In the first column rate constants $k_{ISC} / 10^8 \cdot s^{-1}$ calculated with the original energy gaps are given. The italic numbers represent rate constants for shifted T3 energies ($k_{ISC}^{+0.1\text{ ev}} / 10^8 \cdot s^{-1}$). The factors in the last row represent a measure for the sensitivity of the transition on the energy gap.

Flavin	k_{ISC}	$k_{ISC}^{+0.1\text{ ev}}$	$\frac{k_{ISC}}{k_{ISC}^{+0.1\text{ ev}}}$
MIA	2.7	<i>1.4</i>	1.9
6F	1.6	<i>0.6</i>	3.0
7F	2.6	<i>0.4</i>	7.4
8F	4.4	<i>2.3</i>	1.9
9F	3.2	<i>1.7</i>	1.8

10 Vertical absorption spectra

The line styles depict the main orbital contribution (S1 and T1: $\pi_H \rightarrow \pi_L$, T3 and S5: $\pi_{H-1} \rightarrow \pi_L$, T2 and S3: $n_{N2} \rightarrow \pi_L$, S2: $n_{O2} \rightarrow \pi_L$).

Gas phase

For the relaxation paths in vacuum T1, T2, T3 as well as S2 are considered for the deactivation of the populated S1 state.

10.1 S0

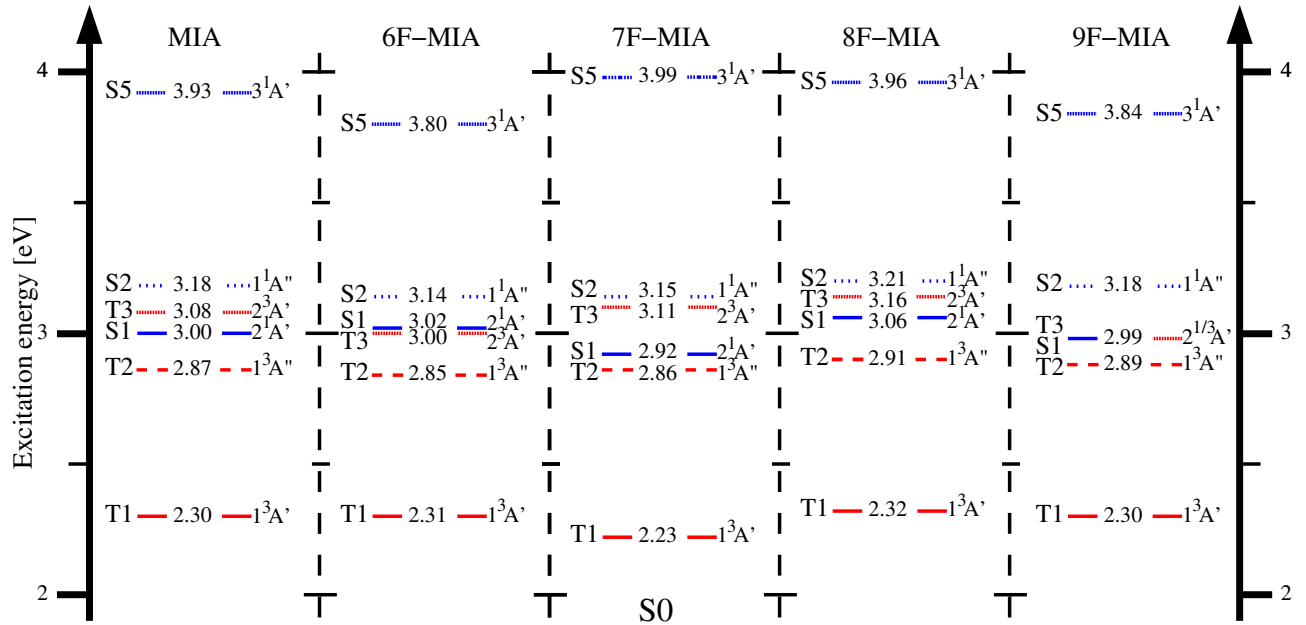


Figure S3: Selected vertical electronic transition energies in eV (DFT/MRCI) at the respective ground state geometries in gas phase.

10.2 S1

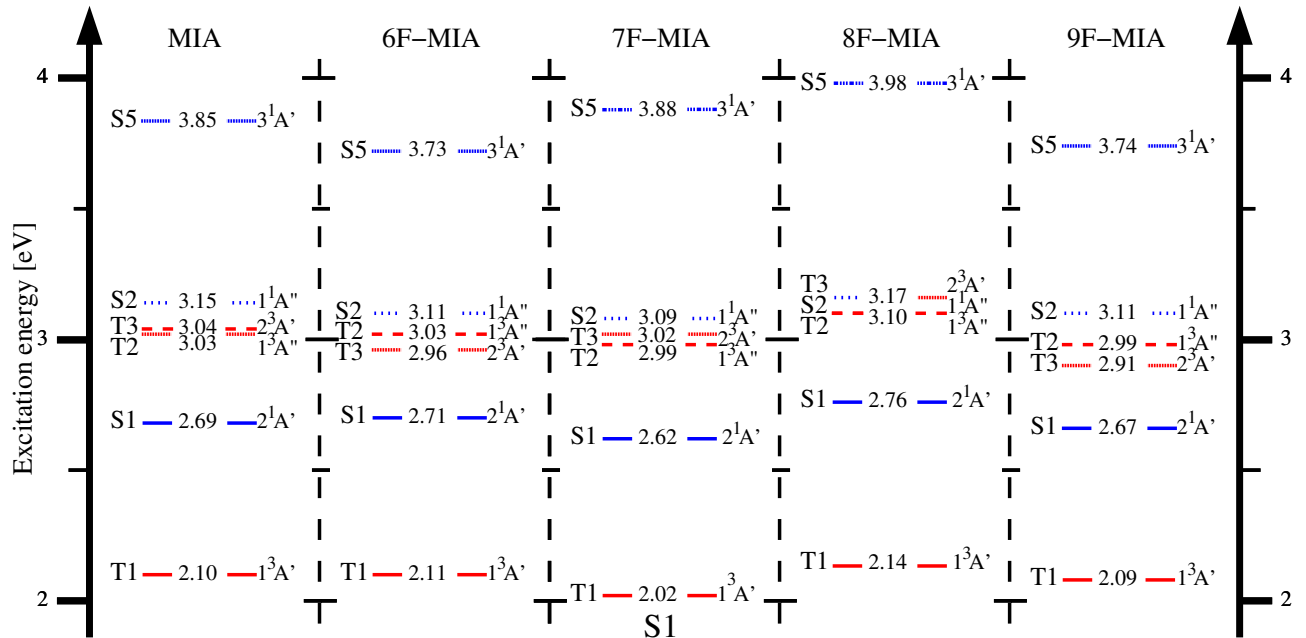


Figure S4: Selected vertical electronic transition energies in eV (DFT/MRCI) at the respective S1 equilibrium geometries in gas phase.

10.3 S2

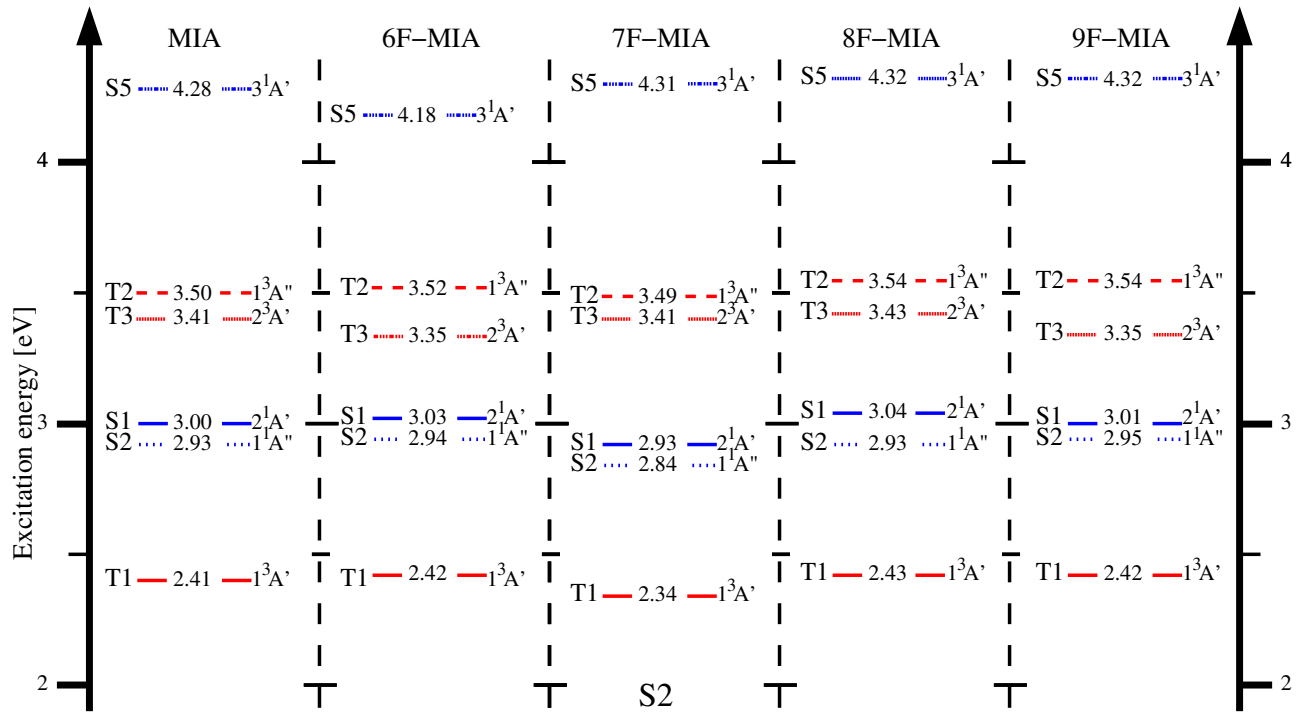


Figure S5: Selected vertical electronic transition energies in eV (DFT/MRCI) at the respective S2 equilibrium geometries in gas phase.

10.4 T1

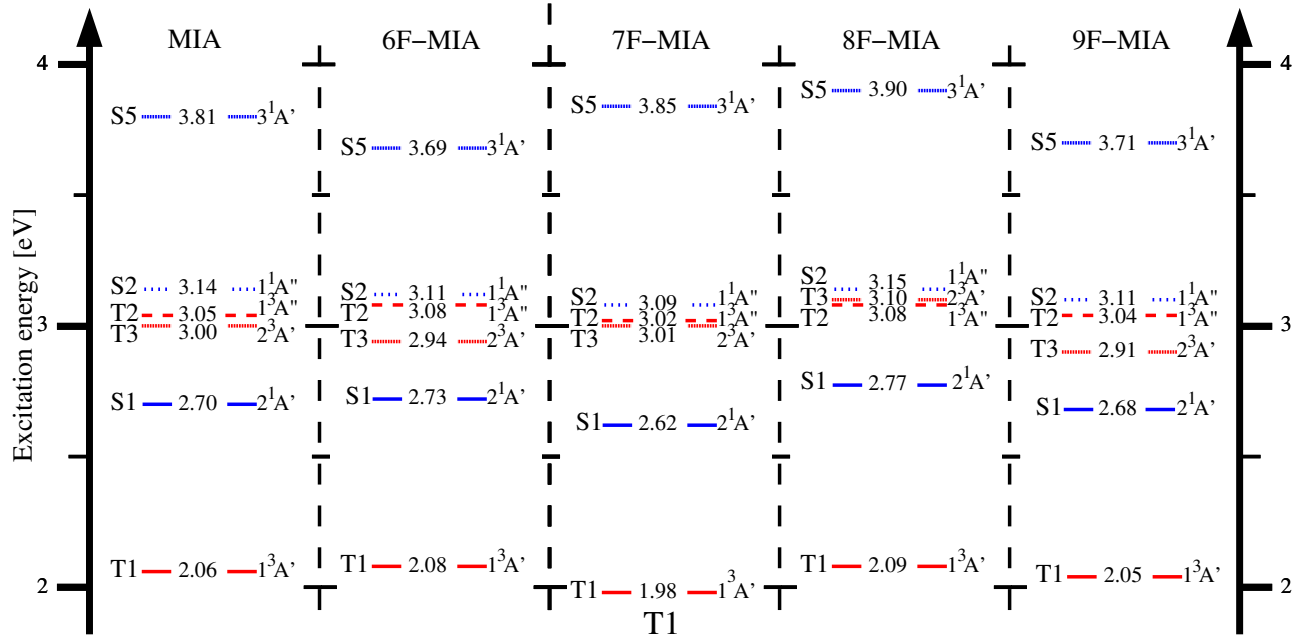


Figure S6: Selected vertical electronic transition energies in eV (DFT/MRCI) at the respective T1 equilibrium geometries in gas phase.

10.5 T2

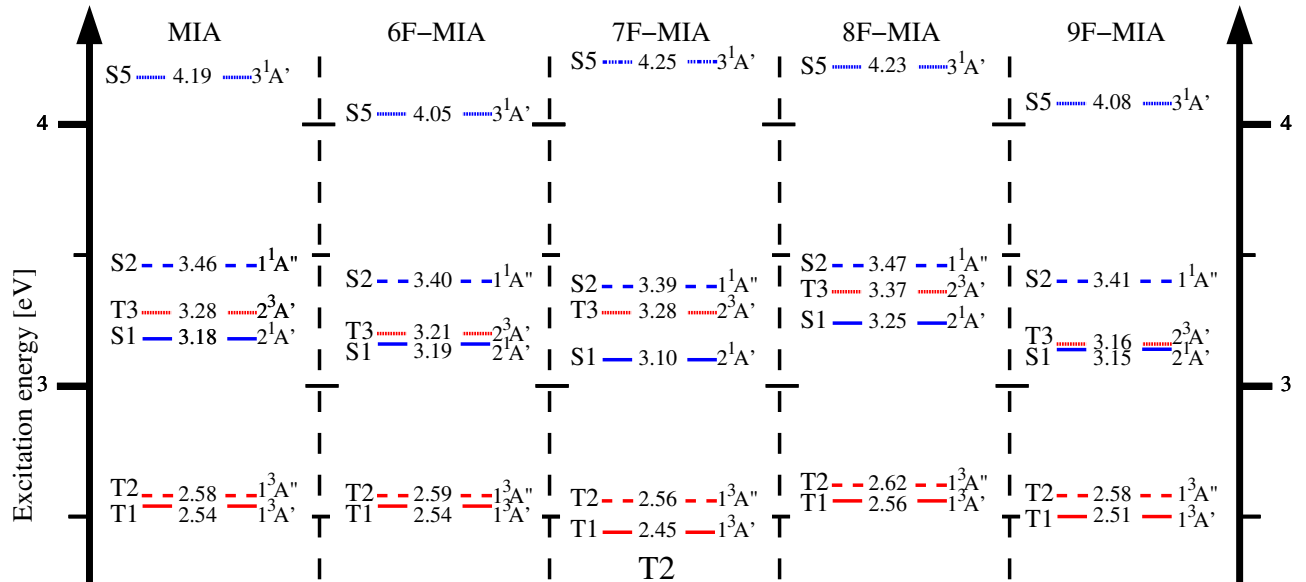


Figure S7: Selected vertical electronic transition energies in eV (DFT/MRCI) at the respective T2 equilibrium geometries in gas phase.

10.6 T3

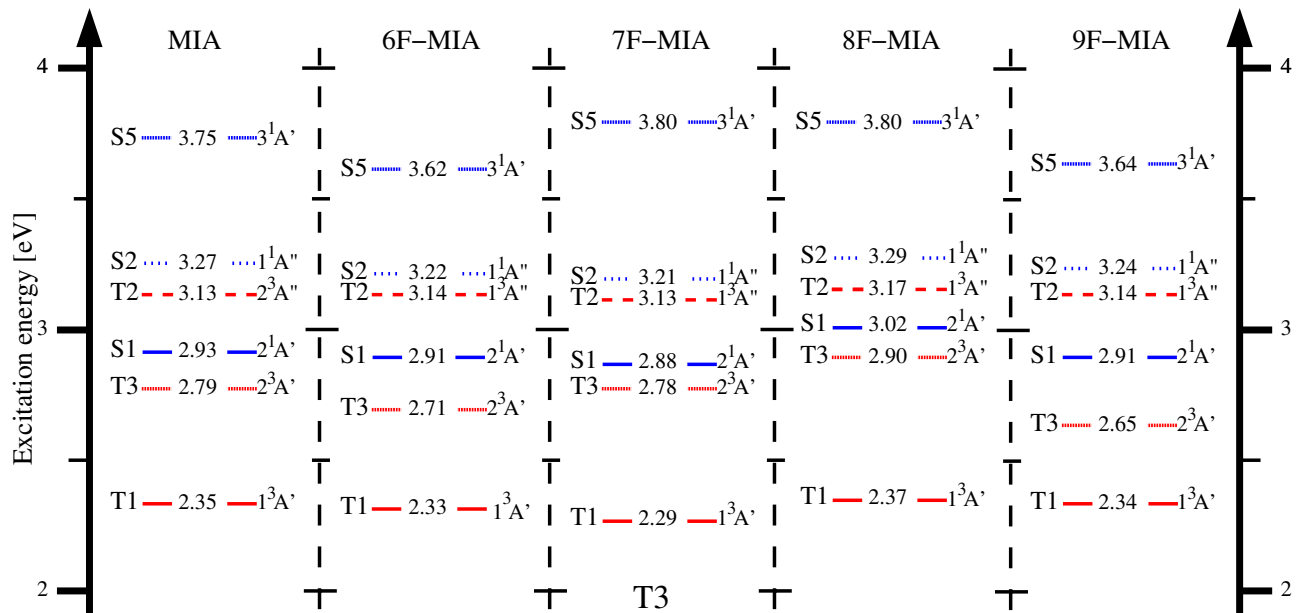


Figure S8: Selected vertical electronic transition energies in eV (DFT/MRCI) at the respective T3 equilibrium geometries in gas phase.

Aqueous medium

$(n\pi^*)^1$ -states are strongly blue shifted in aqueous medium, so that the S2 minimum potential is excluded from the investigation.

Model A

10.7 Ground state

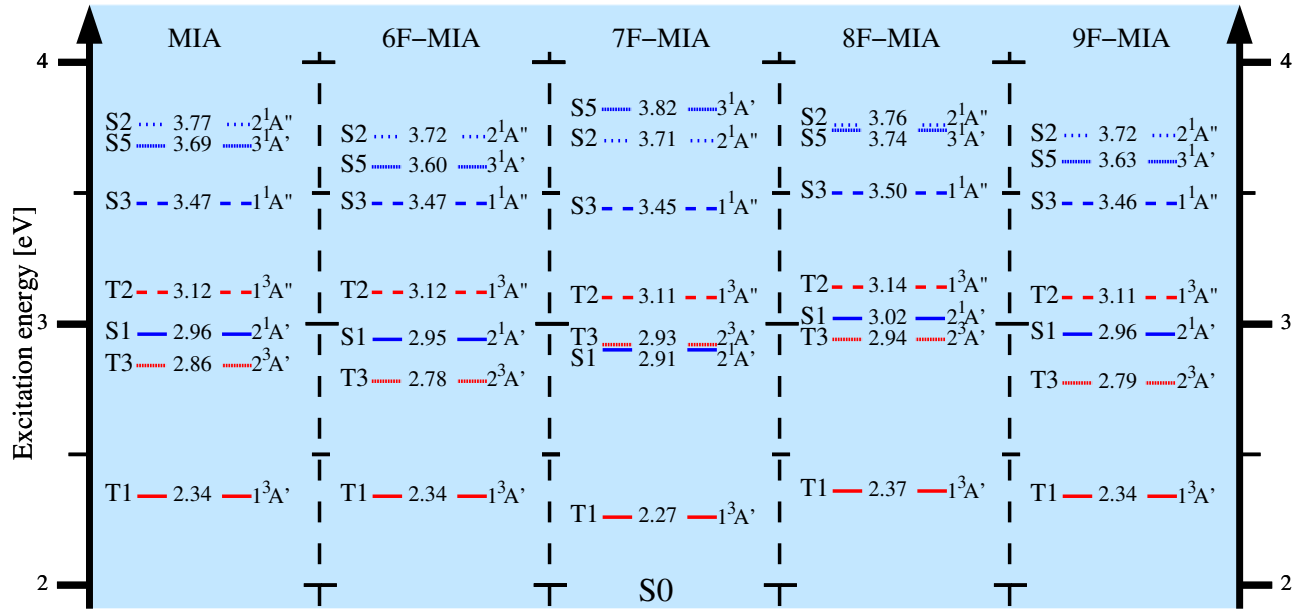


Figure S9: Selected vertical electronic transition energies in eV (DFT/MRCI) at the respective ground state equilibrium geometries in aqueous medium (model A).

10.8 S1

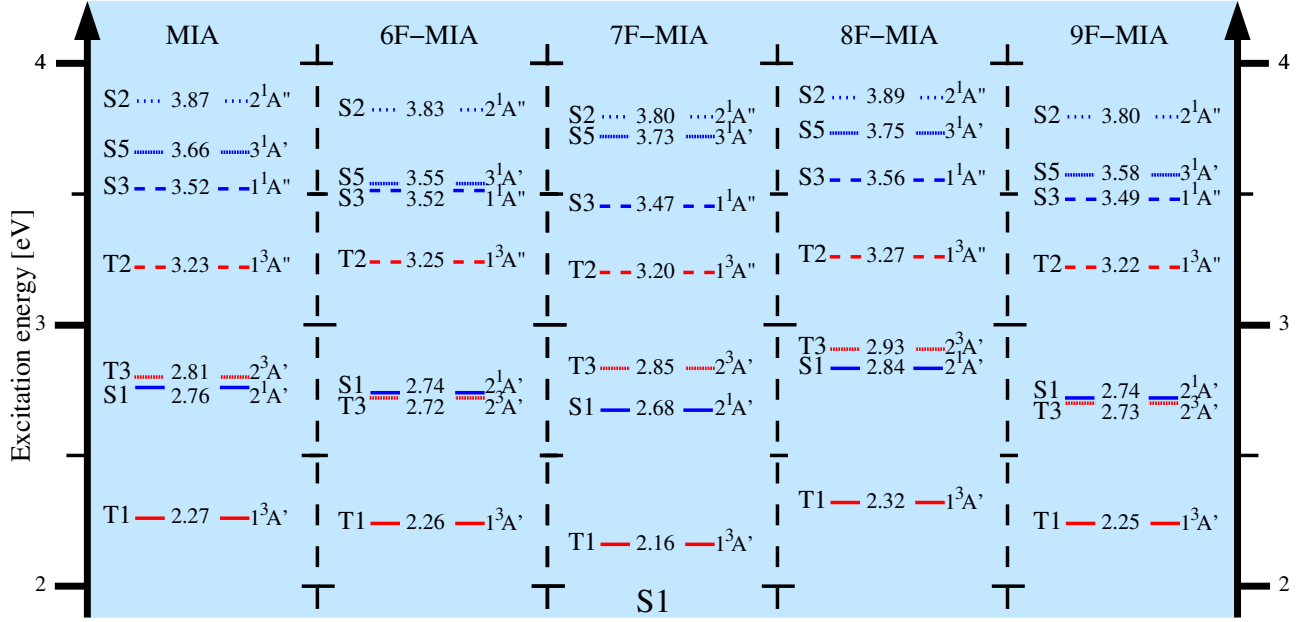


Figure S10: Selected vertical electronic transition energies in eV (DFT/MRCI) at the respective T1 equilibrium geometries in aqueous medium (model A).

10.9 T1

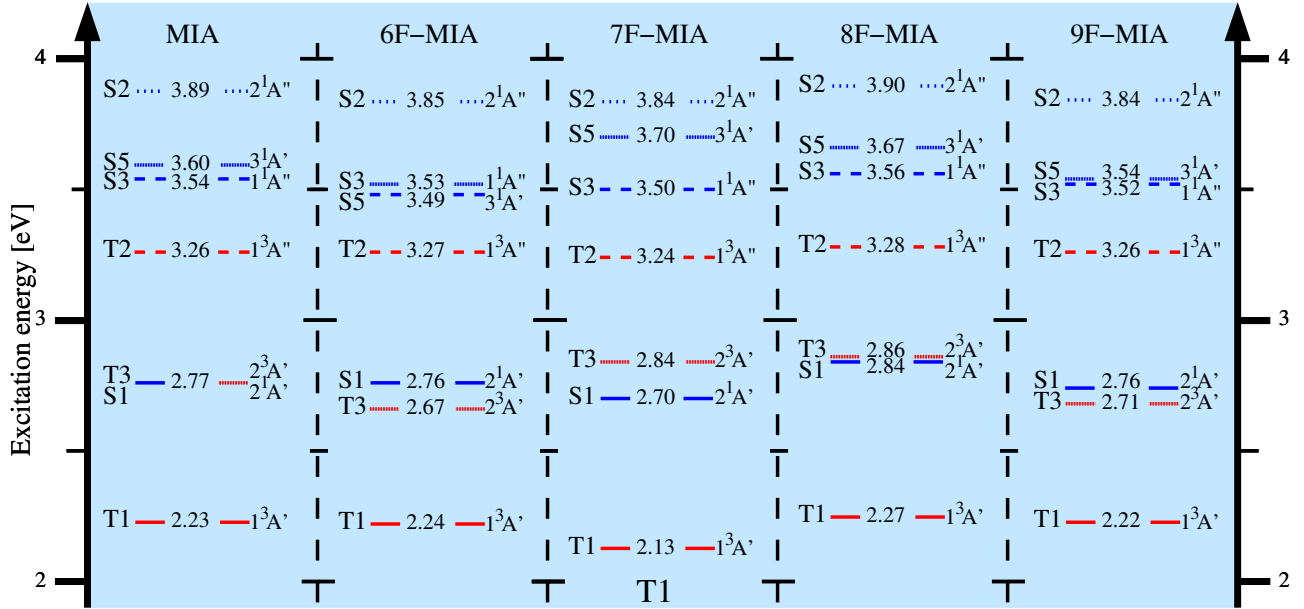


Figure S11: Selected vertical electronic transition energies in eV (DFT/MRCI) at the respective T1 equilibrium geometries in aqueous medium (model A).

10.10 T2

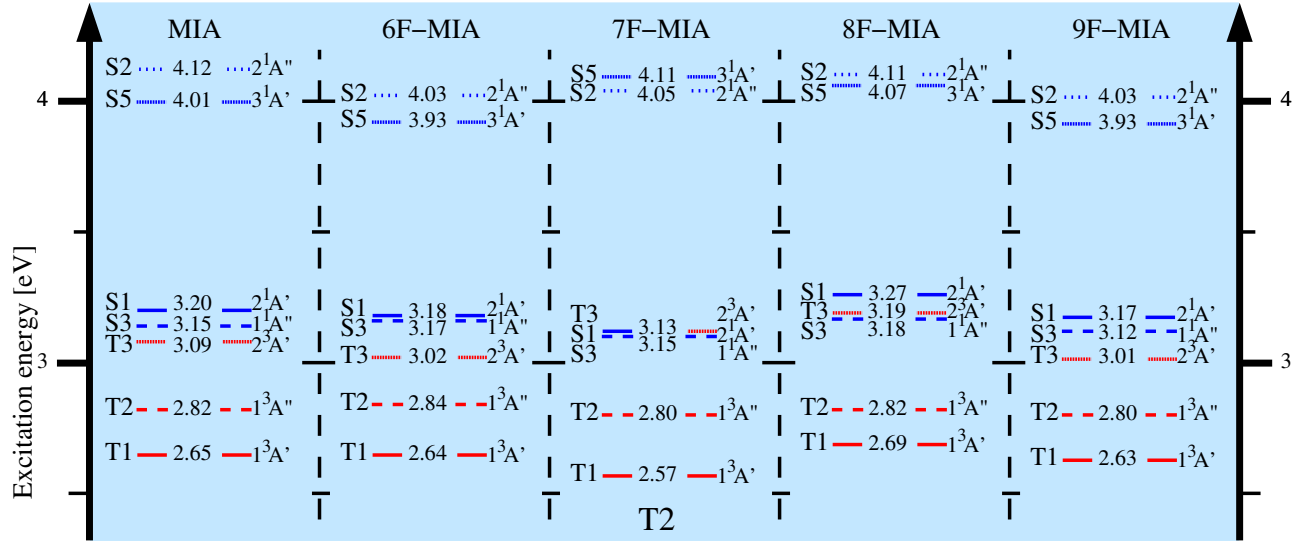


Figure S12: Selected vertical electronic transition energies in eV (DFT/MRCI) at the respective T3 equilibrium geometries in aqueous medium (model A).

10.11 T3

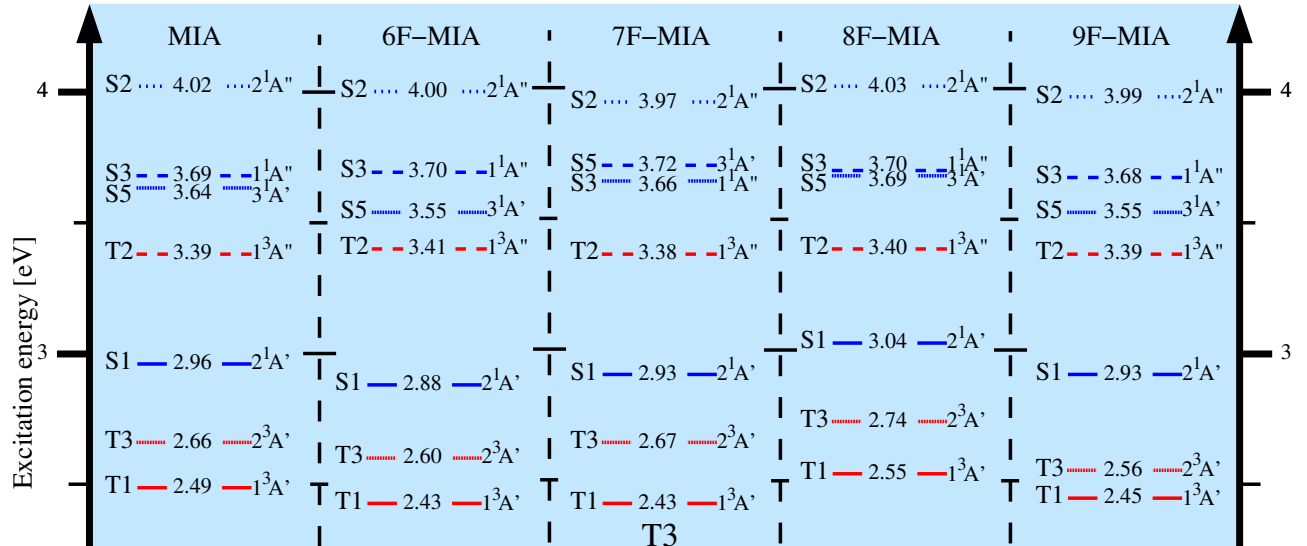


Figure S13: Selected vertical electronic transition energies in eV (DFT/MRCI) at the respective T3 equilibrium geometries in aqueous medium (model A).

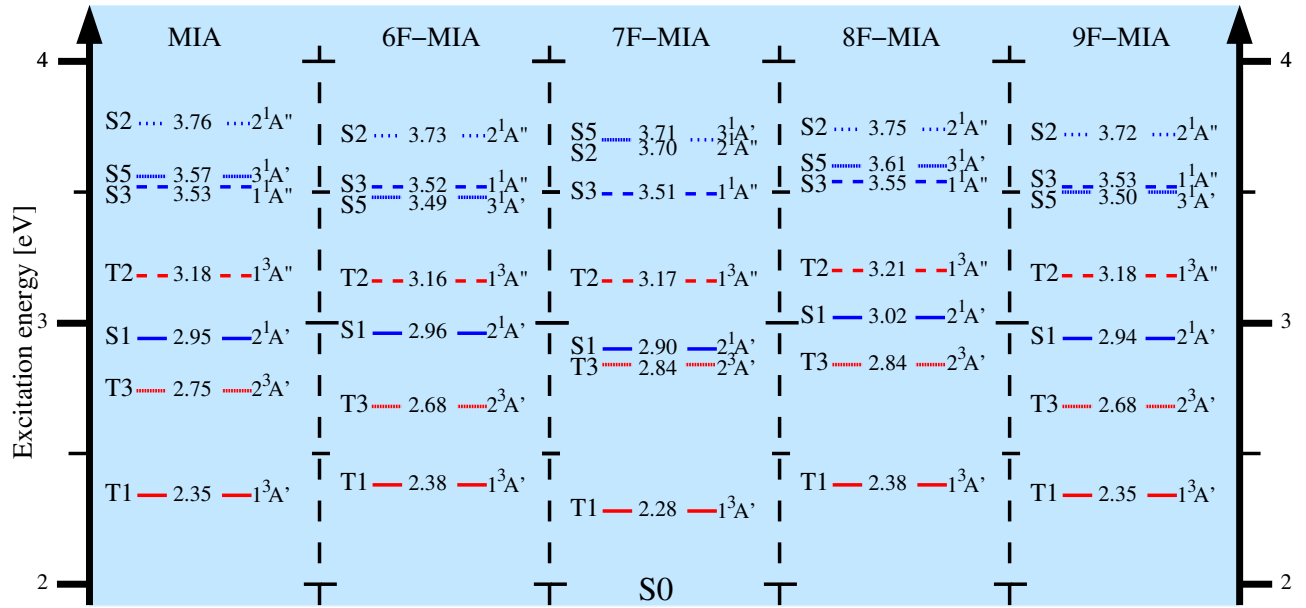
Model B**10.12 Ground state**

Figure S14: Selected vertical electronic transition energies in eV (DFT/MRCI) at the respective ground state equilibrium geometries in aqueous medium (model B).